Chapter 2
Features Based on Triplet Half-Band Wavelet Filter-Banks

Abstract This chapter presents the design of a new class of triplet half-band filter bank (THFB) and investigates its properties to extract iris image features. The feature extraction process and post-classifier have been discussed in this chapter.

Keywords Iris recognition · *k-out-of-n:A* classifier · Post-classifier · THFB · Wavelets

2.1 Introduction

This chapter presents the design of a new class of triplet half-band filter bank (THFB) and investigates its properties to extract the iris image features. The feature extraction process and the post-classifier have been discussed in this chapter.

Daugman [1] used multi-scale quadrature 2-D Gabor filter to demodulate phase information of an iris image to create IrisCode for the authentication. Proenca and Alexandre [2] partitioned normalized iris image into six regions and obtained six IrisCodes using Gabor filters. The matching scores of these six regions are fused together to generate an overall matching score. However, Gabor basis provides an over-complete representation which increases the redundancy and thus time required for iris feature extraction is high. Masek [3] introduced the Log-Gabor filter to encode the phase information of an iris image. Vatsa et al. [4] derived two types of distinct iris features (Log-Gabor and Euler numbers) from the normalized iris images and improved the recognition accuracy by effective segmentation technique, quality enhancement, and SVM rule. However, it consists of many stages to improve the performance. Boles and Boashash [5] used 1-D WT to compute the zero-crossing representation at different resolution levels of a concentric circle on an iris image. However, this method provides very less information along a virtual circle on the iris which affects the recognition accuracy. Wildes [6] obtained the characterization of iris texture through Laplacian pyramid with four different resolution levels. Furthermore, image registration technique is used to align the feature vectors of two iris images and compared the corresponding feature vectors using a normalized

A. D. Rahulkar and R. S. Holambe, *Iris Image Recognition*,
SpringerBriefs in Signal Processing, DOI: 10.1007/978-3-319-06767-4_2,

correlation. However, this registration technique significantly increases the computational complexity of the entire method. Lim et al. [7] used 2-D Haar WT to decompose an iris image into four levels and encoded the fourth-level high-frequency information into an 87-bits binary ordinal code depending upon the sign of the filtered results. However, this method looses middle frequency components of the iris. Ma et al. [8] extracted the texture features of an iris using a bank of spatial filters and used quality descriptor, bootstrap learning and FLD to improve the recognition rate. However, this method is not suitable to perform well in the presence of eyelids/eyelashes occlusion. The same authors used 1-D quadratic spline WT along the angular direction of a normalized iris image [9]. In their work, feature vectors derived based on the local sharp variation points of a variable length called as shape code (SC). Nabti et al. [10] presented multi-resolution iris feature extraction technique by analyzing the iris using first wavelet maxima components and then applying a special Gabor filter bank on the normalized iris image to extract all dominant features. Velisavljević [11] presented iris coding and recognition using directionlets based on 9/7 bi-orthogonal wavelet basis. Abhyankar and Schuckers [12] introduced biorthogonal wavelet neural network (BWN) for off-angle iris recognition by adjusting non-ideal factors through repositioning the BWN. Monro et al. [13] presented ordinal encoding scheme based on the difference of optimized DCT coefficients of overlapped angular patches from normalized iris image. Sun and Tan [14] presented OMs for iris feature representation scheme based on MLDFs using 2-D Gaussian filters. MLDF has been used on 1,024 densely sampled image regions to obtain 1024 bits ordinal code for every iris image with flexible interlobe distance (d). This method has achieved the good trade-off between distinctiveness and robustness. However, this representation may lose some image specific information. Dong et al. [15] introduced a personalized iris matching strategy using a class-specific weight map learned from the training images of the same iris class. The robustness of the weight map totally depends upon the number of training images within a class. However, this method requires more number of training images to decide an effective weight-map within a class which leads to increase the computational cost. Kumar and Passi [16] presented a comparative study of the iris recognition performance using Log-Gabor, Haar wavelet, DCT, and FFT based phase ordinal encoding with small number of training images. Huang et al. [17] introduced a rotation invariant approach for iris feature extraction scheme based on non-separable wavelet FB and Gaussian Markov random field (GMRF). In their work, non-separable wavelet is constructed by using centrally symmetric orthogonal matrices to obtain the iris features in eight different directions. Furthermore, FLD with polynomial kernel is used to improve the computational efficiency and classification accuracy. Park et al. [18] noticed the importance of capturing directional information in iris images where a DFB is applied to a band-pass filtered iris images to derive feature vectors.

It is observed that most of these iris recognition algorithms are sensitive to iris segmentation (detection of inner and outer boundaries). The noise due to inaccurate detection of outer boundary can be easily removed, but the inaccurate detection of pupillary boundary plays a very important role for the iris verification. Due to the inaccurate detection of pupillary boundary, either iris information will lose or

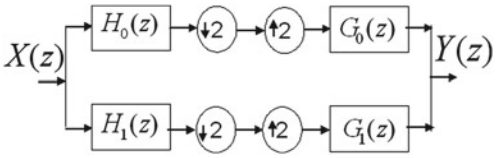

Fig. 2.1 Block diagram of two-channel PRFB

occlusion of pupil will occur on the normalized iris. Thus, an accurate segmentation of iris region is significantly important for iris recognition which may not be possible in the practical iris recognition system. The great progress has been made on iris feature representation, but it is still an open problem. *Although, there is a defined standard for raw iris data, but there is none regarding iris features representation* [14]. Most of the iris feature extraction techniques in the literature used off-the-shelf wavelet basis to extract the iris features. However, many issues are still open in the field of iris feature-extraction and the choice of FB. The design of FB and investigations of their properties (near-orthogonality, regularity, time-frequency localization, linear phase, etc.) for image-coding, denoising, compression, etc. have been carried by many researchers. However, effectiveness of these properties in iris pattern recognition is not addressed in the literature. Hence, this chapter introduces a new wavelet basis for iris texture representation in an attempt to extract effective and compact iris features, and a flexible post-classifier *k-out-of-n:A* so as to handle possible artifacts especially segmentation error (inaccurate detection of inner and outer boundaries of iris), occlusion of eyelids/eyelashes, reflection on iris, shadow of upper/lower eyelid on iris, non-linear deformation, etc.

2.2 Review of the Related Filter Banks

The block diagram of two channel Filter Banks (FB) is shown in Fig. 2.1. The necessary and sufficient conditions for PR are given by the following two equations:

$$H_0(z)G_0(z) + H_0(-z)G_0(-z) = 2, \tag{2.1}$$

$$H_1 = z^{-1}G_0(-z), \quad G_1(z) = zH_0(-z). \tag{2.2}$$

The product filter $P(z) = H_0(z)G_0(z)$ in Eq. (2.1) belongs to the special class of filters known as half-band filter. The analysis scaling and wavelet functions are given by the following two-scale dilation equations:

$$\phi(t) = \frac{2}{|H_0(\omega)|_{\omega=0}} \sum_n h_0(n)\phi(2t-n), \tag{2.3}$$

$$\psi(t) = \frac{2}{|G_0(\omega)|_{\omega=0}} \sum_n h_1(n)\phi(2t-n). \tag{2.4}$$

where $h_0(n)$ and $h_1(n)$ are the analysis low-pass filter (LPF) and high-pass filter (HPF) coefficients respectively.

The two-channel wavelet FBs have been widely used in many applications which require signal decomposition e.g. pattern recognition, compression, super-resolution, etc. The biorthogonal FBs preferred for image processing due to its symmetric scaling and wavelet functions. Regularity of wavelets is an important property which imposed in the design of wavelet filters by having vanishing moments (zeros at $z = -1$) at the aliasing frequencies of wavelet HPFs. Meanwhile, one of the design characteristics of wavelet FBs for signal analysis is the ability to achieve time-frequency localization. Thus, it is desirable to design a wavelet FBs that fulfill PR, linear phase, orthogonality, regularity and time-frequency localization. One of the most common design methods for designing wavelet filters is the factorization of a HBP [19]. It is well known that most of the popular biorthogonal FBs (e.g. Cohen-Daubechies-Feauveau (CDF-9/7), spline family of wavelet FBs [20–22] are designed by the factorization of a Lagrange half-band polynomial (LHBP). The LHBP has the maximum number of zeros at $z = -1$ to achieve the maximum regularity.

However, LHBP filters do not have any degree of freedom and thus there is no direct control over frequency response of the filters. In order to have some independent parameters (which can be optimized to obtain some control over frequency response of the filter), Patil et al. [19] used general half-band filter factorization (not LHBP) to design two-channel bi-orthogonal wavelet FIR FBs (BWFB). However, it is observed that this factorization (includes decision of factorization of remainder polynomial and reassignment of zeros) improves the frequency response of one of the filters (analysis/synthesis) at the cost of the other filter (synthesis/analysis). The improvement in frequency response of both the filters heavily depends upon the factorization of a HBP. This is somewhat tedious task for higher order HBPs. It is also observed that the designed biorthogonal FBs lose "maximal flat" condition and it is far away from orthogonality condition. Lifting scheme is also one of the attractive schemes to design wavelet FBs that provides structurally imposed PR property [23]. Based on the lifting scheme, Phoong et al. [24] introduced a class of halfband pair filterbank (HPFB) structure based on two kernels. In HPFB structure, magnitudes of the frequency responses of the analysis and synthesis low pass filters at $\omega = \pi/2$ are restricted to 0.5 and 1.0 respectively or vice-versa. This encounters certain restrictions for the control of its frequency response. In order to overcome this restriction [24], Ansari et al. [25] proposed a FB structure based on a class of THFB using three kernels that have structural PR, feature-rich structure and simple design. In their work, two methods are proposed to design two-channel 1-D biorthogonal FBs based on the triplet of half-band filters. The first method is based on Lagrange filter coefficients to achieve maximal flatness in the filters (due to maximum regularity) with slow frequency roll-off. The second method is employed Remez algorithm which results in equiripple filters with user-defined cut-off frequencies. It has sharp frequency roll-off but does not have the regularity condition. In their work, the shape parameter p is used to achieve a greater flexibility in frequency response of the filters. However, regularity order related to the number of zeros at $z = -1$ has not been specified. In order to bridge the gap between these two extremes, Tay and Palaniswami [26] introduced a novel approach to design a class of THFB. Parametric Bernstein polynomial is used to impose the required vanishing moments (VMs). This technique is based

on iterative least square approach to determine the coefficients of Bernstein polynomial. However, Bernstein polynomial is suitable for nearly maximally flat frequency response rather than for ripple responses with sharp roll-off. In [27], Tay modified the work of [26] and suggested a new class of even-length biorthogonal wavelet filters for Hilbert pair design (ETHFB). Chan and Yeung [28] presented a design of THFB with regularity using semi-definite programming (SDP). However, the semi-infinite constraints are approximated by a large finite number of constraints that give an inefficient design for higher order filters. Kha et al. [29] proposed an efficient SDP method in order to design a class of THFB with optimal frequency selectivity for a given regularity condition. Eslami and Radha [30] generalized Ansari's method to a multidimensional FB design with any number of analysis and synthesis VMs using a structural approach based on Kovacevic method [31]. The filters designed in [30] achieved better regularity, lower frame bounds and better frequency selectivity than the filters designed in [31].

In this chapter, a new class of THFB is designed in order to overcome the limitations of recently presented FBs in [19, 25]. Firstly, three kernels are designed from the generalized HBP by imposing the zeros at $z = -1$. These three designed kernels are used in three step ladder structure to design a new class of THFB by varying the shape parameter p. The objective function involves optimization of frequency response of the filters. We have also shown that the designed filters achieve better frequency selectivity, near-orthogonality, good time-frequency localization with linear phase and PR condition. This FB is used to form a new wavelet basis for extracting the textural features of an iris image.

2.2.1 Triplet Halfband Filter Bank

The analysis and synthesis LPFs of a class of Triplet Halfband Filter Bank (THFB) consist of three kernels as follows [25] :

$$H_0(z) = \frac{1+p}{2} + \left(\frac{1+p}{2}\right) zT_1(z^2) \left(\frac{1-pzT_0(z^2)}{1+p}\right), \tag{2.5}$$

$$G_0(z) = \frac{1+pzT_0(z^2)}{1+p} + \frac{1-p}{1+p} zT_2(z^2) H_0(-z). \tag{2.6}$$

where, $T_m(z)$ is obtained using:

$$T_m(z) = \sum_{n=1}^{N \in even} t_m(n)(z^{-n} + z^{n-1}), \quad m = 0, 1, 2$$

The three HBPs $T_0(z^2)$, $T_1(z^2)$, and $T_2(z^2)$ required for Eqs. (2.5) and (2.6) are obtained using upsampled by 2 operation as:

$$zT_m(z^2) = \sum_{n=1}^{N_m \in even} t_m(n)(z^{-2n+1} + z^{2n-1}), \quad m = 0, 1, 2. \tag{2.7}$$

and the coefficients $t_m(n)$ are obtained using standard Lagrange interpolation formula as:

$$t_m(n) = \frac{(-1)^{n+N_m-1} \prod_{\iota=1}^{2N_m} (N_m + 1/2 - \iota)}{(N_m - n)!(N_m - 1 + n)!(2n - 1)}$$

The analysis and synthesis HPFs are obtained from Eq. (2.2) by quadrature mirroring the LPFs. This class of THFB is implemented using three-step ladder structure. The parameter p (degree of freedom) provides some flexibility in order to set the same magnitude of the frequency response at $\omega = \pi/2$ for both the analysis and synthesis LPFs (symmetry between analysis and synthesis filters).

2.2.2 Factorization Based on a Generalized Half-Band Polynomial

The alternate approach to the design of two-channel FBs is the design of a halfband filter, followed by its factorization to derive analysis and synthesis LPFs. Regularity imposed in the design of $P(z)$ by introducing zeros at $z = -1$. Patil et al. [19] presented an approach to design FIR wavelet FBs using factorization of a half-band polynomial (HBP). This approach is briefly discussed as follows:

1. Assume generalized symmetric half-band polynomial $P(z)$ of order K as

$$P(z) = a_0 + a_2 z^{-2} + \cdots + a_{\frac{K}{2}-1} z^{-\frac{K}{2}-1} + z^{-\frac{K}{2}} + a_{\frac{K}{2}-1} z^{-\frac{K}{2}+1} + \cdots + a_0 z^{-K}$$

   The coefficients a_k (degree of freedom) of $P(z)$ have to be designed.
2. Obtain L constraints on the coefficients a_k of $P(z)$ by introducing L zeros at $z = -1$.
3. Using these constraints, $P(z)$ can be expressed in terms of the independent (free) parameters.
4. Now express the polynomial $P(z)$ as $P(z) = (z + 1)^L R(z)$, where $R(z)$ is the remainder polynomial. Next factorize this $R(z)$ into $R_1(z)$ and $R_2(z)$ to obtain final filters as $H_0(z) = (z + 1)^{L/2} R_1(z)$ and $G_0(z) = (z + 1)^{L/2} R_2(z)$.
   The independent coefficients are obtained by optimizing the objective function (frequency responses of the factored filters $H_0(z)$ and $G_0(z)$). It is observed that the improvement in frequency responses of both the filters $H_0(z)$ and $G_0(z)$ is totally depend on the step 4.

2.3 Design of New Class of THFB

In this chapter, a new class of THFB is formulated in order to avoid the factorization process and improve the frequency response of both the filters simultaneously. First, general HBP of an order K (expressed in coefficients a_k) which offers $(\frac{K}{2}+1)$ degrees of freedom to impose the vanishing moments is considered. From this polynomial, three HBPs $P_1(z)$, $P_2(z)$, and $P_3(z)$ are obtained by imposing M zeros at $z=-1$, where $M<(\frac{K}{2}+1)$. With this, desired number of independent parameters a_k (degree of freedom) are obtained without imposing maximum flatness constraint. These three HBPs can be expressed as follows:

$$P_i(z) = (z^{-1}+1)^{M_i} R_i(z), \quad i = 1, 2, 3. \tag{2.8}$$

where M_i is the number of zeros at $z=-1$ for ith polynomial and the remainder term $R_i(z)$ is given by the following equation:

$$R_i(z) = a_0 + c_1 z^{-1} + c_2 z^{-2} + \cdots + a_0 z^{K-M_i} \tag{2.9}$$

where c_j are the constants which can be expressed as functions of a single parameter a_0 (as given in Eq. (2.9)). Thus, three remainder polynomials $R_1(z)$, $R_2(z)$, and $R_3(z)$ are obtained by imposing M_1, M_2, and M_3 (where $M = M_1 + M_2 + M_3 = \frac{K}{2}$ can be a choice) zeros on $P(z)$ (of order K). It may be noted that the remainder polynomials can also be expressed into any desired number of independent or free parameters $(a_0, a_2, a_4, \ldots)$. Expressing the c_j (remainder polynomial) with more number of a_k provides better flexibility at the cost of computational complexity. With this, these three HBPs provide one degree of freedom (independent parameters) by which flexibility in frequency responses can be achieved. We can also construct three kernels from three different HBPs. In this context, any desired values of M_1, M_2, and M_3 can be used and available degrees of freedom are utilized to tweak the frequency response. The required class of three kernels given in Eq. (2.7) is obtained by following equation

$$\begin{aligned} T_0(z^2) &= z^{K/2} P_1(z) - 1; \\ T_1(z^2) &= z^{K/2} P_2(z) - 1; \\ T_2(z^2) &= z^{K/2} P_3(z) - 1. \end{aligned}$$

These three designed kernels are then used in the three-step lifting scheme to obtain a new class of analysis and synthesis LPFs respectively as follows:

$$H_0(z) = \frac{1+p}{2} + \frac{1+p}{2}\left(z^{K/2}P_2(z) - 1\right)\left(\frac{1}{1+p}\left(1 + p\left(1 - z^{K/2}P_1(z)\right)\right)\right), \tag{2.10}$$

$$G_0(z) = \frac{1 - p + pz^{K/2}P_1(z)}{1 + p} + \left(\frac{1 - p}{1 + p}\right)\left(z^{K/2}P_3(z) - 1\right)H_0(-z). \quad (2.11)$$

where, K is the order of HBP. The use of a class of THFB provides one more degree of freedom (p) by which we can shape better frequency responses of the final filters. Thus, the suggested design offers more flexibility in the design of filters using two degrees of freedom (a_k and p). This method has been illustrated in Sect. 2.3.1 with one example. Due to the use of THFB and general HBP, frequency responses of both the filters have been improved simultaneously. These filters satisfy regularity, near-orthogonality, linear-phase, and PR properties. The resulting lengths of the analysis LPF $H_0(z)$ is $N_1 + N_2 - 1$ and synthesis LPFs $H_0(z)$ is $N_1 + N_2 + N_3 - 2$, where N_1, N_2, and N_3 are the lengths of $P_1(z)$, $P_2(z)$, and $P_3(z)$ respectively. It is observed that synthesis LPF $G_0(z)$ is long and smooth as compared to synthesis HPF $G_1(z)$. This setting is more desirable to avoid blocking, checkerboard, and ringing artifacts during signal reconstruction in lossy coding [32].

2.3.1 Design Example

In the following example, 6th order HBP is used to design the required kernels $T_0(z^2)$, $T_1(z^2)$, and $T_2(z^2)$.

Example: Consider $P(z)$ of order 6

$$P(z) = a_0 + a_2z^{-2} + z^{-3} + a_2z^{-4} + a_0z^{-6}. \quad (2.12)$$

This $P(z)$ is used to construct $P_1(z)$, $P_2(z)$, and $P_3(z)$ by imposing the zeros at $z = -1$ with the help of synthetic-division such that these three polynomials can be expressed in terms of a single independent parameter a_0. Consider $M_1 = 0$, $M_2 = 1$, and $M_3 = 2$ such that $M_1 + M_2 + M_3 = M = 3$, where $M < (\frac{K}{2} + 1)$.

The polynomials are expressed as follows:

$$\begin{aligned}
P_1(z) &= a_0 + (a_0 + 0.5)z^{-2} + (-a_0 + \frac{1}{2})z^{-4} + a_0z^{-6},\\
P_2(z) &= (1 + z^{-1})(a_0 + (-a_0)z^{-1} + \frac{1}{2}z^{-2} + \frac{1}{2}z^{-3} + (-a_0)z^{-4} + a_0^{-5}), \quad (2.13)\\
P_3(z) &= (1 + z^{-1})^2(a_0 + (-2a_0)z^{-1} + (2a_0 + \frac{1}{2})z^{-2} + (-2a_0)z^{-3} + a_0z^{-4}).
\end{aligned}$$

Now optimized value of $a_0 = -0.062499$ is obtained using MATLAB optimization routine *fminunc*. This value of a_0 minimizes the energy in the ripples of these kernels. The proposed transfer functions for the class of THFB are obtained by using Eqs. (2.5) and (2.6) to derive the LP analysis filter $H_0(z)$ and synthesis filter $G_0(z)$. The optimized value of shaping parameter $p = \sqrt{2} - 1$ is used to obtain the same

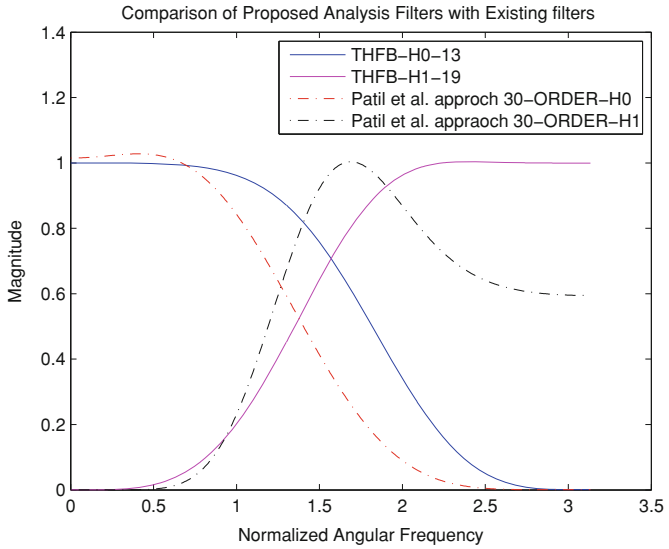

Fig. 2.2 Magnitude responses of the filter bank pair

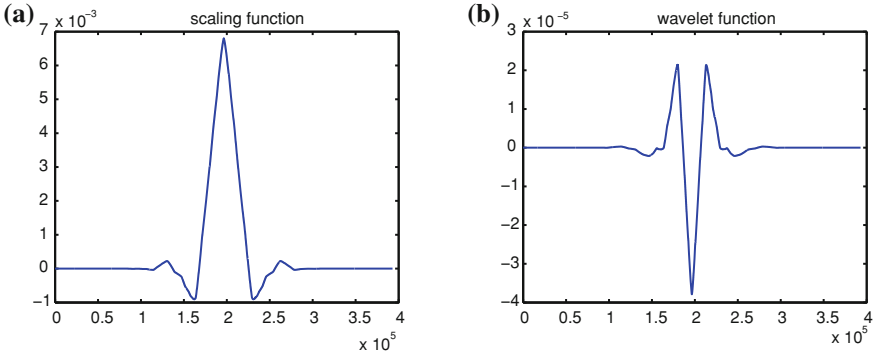

Fig. 2.3 **a** Scaling and **b** Wavelet functions

magnitude of $H_0(z)$ and $G_0(z)$ at $\omega = \pi/2$. The lengths of filters $H_0(z)$ and $G_0(z)$ are 13 and 19 respectively. We compare the results of this proposed FBs with the same length FBs designed using existing approach of [19]. The technique in [19] needs 30th order HBP to get analysis and synthesis LPFs of length 13 and 19 respectively. Fourteen zeros are imposed at $z = -1$ on 30th order HBP. Then six zeros to analysis and eight zeros to synthesis LPFs are reassigned to obtain 13/19 length filters respectively. The frequency responses of the proposed analysis LPF and HPF are compared with the existing FBs [19] as shown in Fig. 2.2. The analysis scaling and wavelet functions for the proposed FBs are shown in Fig. 2.3.

The properties of the proposed FB desirable for iris feature extraction are briefly discussed as follows:

2.3.2 Properties of the Designed THFB Desirable for Iris Feature Extraction

1. **Linear phase (symmetry)**:
   The non-symmetric wavelet basis degrades the classification accuracy due to its non-linear phase. The non-linear phase generates phase distortion and the spatial localization of the wavelet coefficients can not be well-preserved. It can have a major effect on the shape of the output signal which can lead to decrease the texture discrimination capability. Thus, linear-phase plays an important role for iris feature extraction.
2. **Near-orthogonality**:
   Similarity between analysis and synthesis filters is a desirable property. It could be used as a measure of near-orthogonality [30]. It is a quantitative measure of how far a biorthogonal FBs from orthogonality. In this chapter, $\|h_0 - g_0\|^2$ (h_0 and g_0 are LP analysis and synthesis filters coefficients respectively) and $|H_0(\pi/2) - G_0(\pi/2)|$ are used to measure the dissimilarity of the designed filters. Also, it is well known that orthogonality conserves the energy between the input and output of the FB [33]. This property over bi-orthogonality can be useful to represent iris features that can have better bit allocation technique and less distortion due to quantization noise. This property also plays an important role for the texture classification in the presence of noise. The details are presented in [34].
3. **Frequency selectivity**:
   Measure of energy of the error between designed normalized filter and ideal filter is one of the ways to determine frequency selectivity [30]. The total energy of the error is defined as

$$E = \int_{0}^{(\pi/2)} |1 - H_0(\omega)|^2 d\omega + \int_{\pi/2}^{\pi} |H_0(\omega)|^2 d\omega. \tag{2.14}$$

   In this chapter, Eq. (2.14) is used as an objective function to choose the value of a_0. The proposed FB provides good frequency selectivity which is helpful to represent effective iris features.
4. **Regularity**:
   It is well known that one of the important properties of a wavelet FB is regularity. The regularity leads to smooth scaling and wavelet functions. Regularity is imposed in the design of wavelet FB by imposing zeros at $z = -1$ [35]. The LP filtering followed by decimation will result in the aliasing due to the lower

Table 2.1 Properties measures of 1-D analysis LPFs

Properties measures	Patil's FB 30th order	Proposed THFB 13/19
$\|H_0(pi/2) - G_0(pi/2)\|$	0.6318	0.0026
$\|h_0 - g_0\|^2$	57.76	0.1589
E	61.65	59.65
Δt^2	0.5595	0.9464
$\Delta\omega^2$	0.5662	0.5672

sampling rate. Consequently, successively LP filtering with decimation results in more aliasing terms [34]. This leads to produce significant iris verification error. Thus, it is desirable to approximate the iris features in order to minimize the quantization error and have better iris texture discrimination. It is also important to note that if regularity order of analysis wavelet function is greater than the synthesis wavelet function, then the resultant wavelet basis has more approximation power in the decomposition section and is more regular in reconstruction [30]. This setting is more desirable for iris feature extraction.

5. **Time-Frequency localization**:
   Time-frequency localization plays a very important role in order to show the ability of WT for signal analysis. However, many of wavelet design techniques do not explicitly incorporate any localization criteria [36]. The measure of spatial localization and frequency localization are computed directly from filter coefficients. The details are given in [36, 37]. It is also given that lower $\triangle\omega^2$ have a sharper roll-off in the frequency response. The proposed FB provides better time-frequency resolution, so it can be well adopted to characterize the variations in iris images.

Table 2.1 presents the performance measures for some of the properties of the designed filters using approach in [19] and the class of THFB. It is observed that investigated filters provide more similarity between analysis and synthesis LPFs (near-orthogonality), good frequency selectivity, and good time-frequency localization. It may be noted that the designed filters can achieve all the above properties for any order of HBP.

In order to apply investigated class of THFB to iris images, 2-D extension of wavelets are required. An obvious way to construct separable 2-D wavelet filters is to use tensor product of their 1-D counterparts. A 2-D approximation and three detail functions are obtained from Eq. (2.15) as:

$$\begin{aligned} L(z) &= H_0^{1d}(z_1) \times H_0^{1d}(z_2) \\ H(z) &= H_0^{1d}(z_1) \times H_1^{1d}(z_2) \\ V(z) &= H_1^{1d}(z_1) \times H_0^{1d}(z_2) \\ D(z) &= H_1^{1d}(z_1) \times H_1^{1d}(z_2). \end{aligned} \tag{2.15}$$

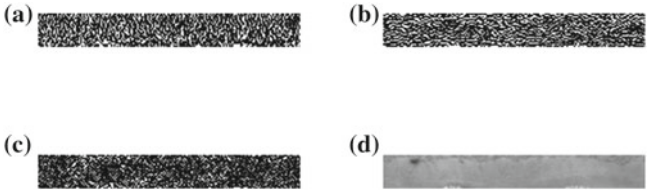

Fig. 2.4 One-level decomposition of CASIA-IrisV3.0 iris image using proposed class of THFB **a** LH sub-band **b** HL sub-band **c** HH sub-band **d** approximate (LL) sub-band

where $H_0^{1d}(z_1)$ and $H_1^{1d}(z_1)$ are 1-D LPF and HPF respectively of the designed filter-banks. The one-level decomposition results in *Vertical* (V), *Horizontal* (H), and *Diagonal* (D) sub-bands and one *approximation sub-band* (L), which corresponds to LH, HL, HH, and LL sub-bands respectively as shown in Fig. 2.4a–d for one of the iris images.

2.4 Iris Recognition Algorithm

In this work, iris features which are mostly oriented in vertical, horizontal and diagonal directions are computed by the introduced wavelet basis. The inner half iris region is divided into six sub-images and selected only four regions for further processing. This new class of THFB is applied separately on each of the four selected sub-blocks (sub-images). The feature vector for each sub-image is derived by estimating the channel energies of the THFB. The four distance scores are obtained and fused by the flexible post-classifier (*k-out-of-n:A*) in order to develop robust iris recognition technique. The block diagram of the half-iris recognition technique is shown in Fig. 2.5.

2.4.1 Feature Extraction Using a New Class of THFB

The original eye image must be preprocessed in order to extract iris features from an eye image. The preprocessing involves localization and normalization of iris image. In this work, iris is localized using Daugman's IDO and normalized with the help of DRSM of the fixed size [1]. The preprocessing steps are shown in Fig. 2.6a–c.

Although some of the existing methods extract iris texture efficiently, their performance degrades significantly when the image quality is poor. Chen et al. [38] suggested that different regions of the iris have different qualities and local iris image regions with better quality have better classification capability and vice-versa. In multi-biometric recognition system, fusion of information extracted from classifiers provide better recognition performance as compared to single classifier

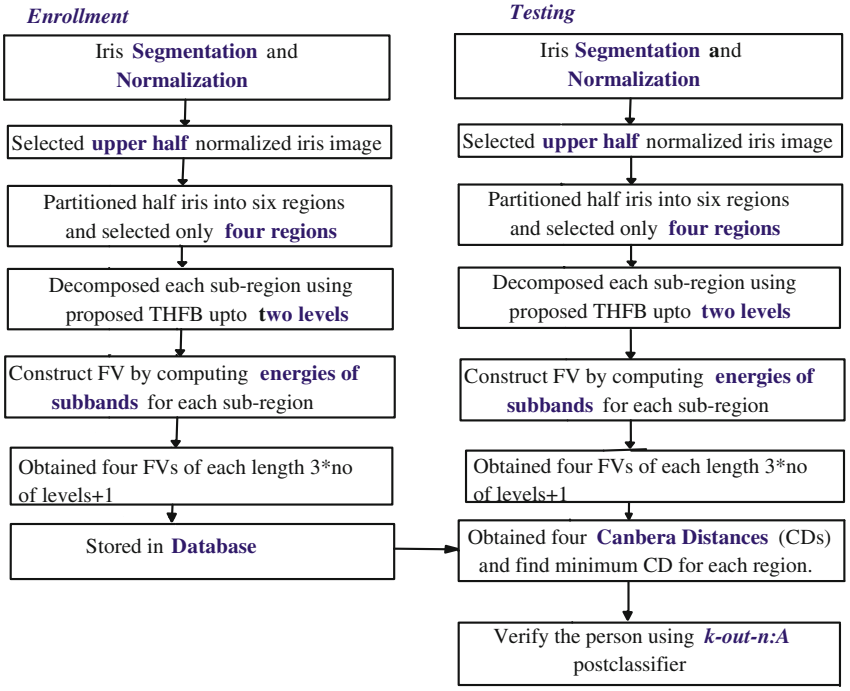

Fig. 2.5 Block diagram of the proposed iris recognition scheme

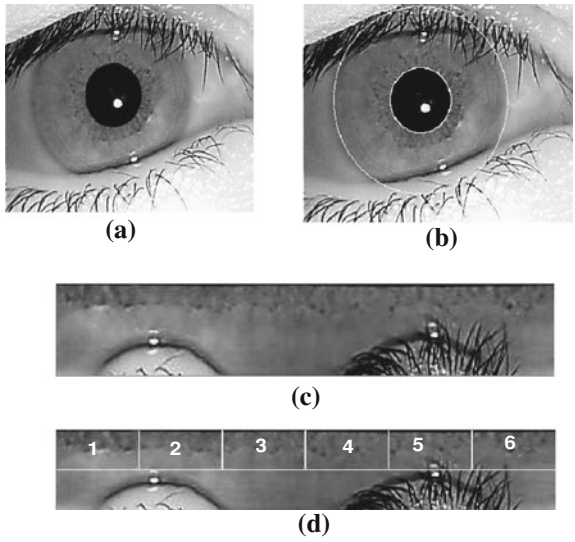

Fig. 2.6 **a** Original eye image. **b** Segmented iris image. **c** Normalized iris image. **d** Partitioned normalized iris image

[2, 4, 39]. Therefore, instead of recognizing the entire iris image, we have divided the iris image into multiple regions. Each iris sub-region is recognized separately and fused the decision using flexible post-classifier. The upper half-iris (inner iris region) is preferred from the entire normalized iris image because (1) the region closer to the pupil provides more discriminating iris information and (2) limbic boundary sometimes may not be segmented properly. Thus, one of the practical artifacts (inaccurate outer-boundary detection) in the iris recognition system has been removed inherently. This half-iris is divided into six sub-regions and selected only four sub-regions (Region: 1, 3, 4, and 6) as shown in Fig. 2.6d so as to minimize some effect of occlusions during iris recognition. The designed wavelets filters are applied on each of these four regions to extract multi-resolution based iris texture. As energy is an important characteristic in identifying texture (which is normally being used in the literature to represent textures), the normalized energy is computed by L_1 norm from each channel of the THFB as below.

$$E_i = \frac{1}{M \times N} \sum_{m=1}^{M} \sum_{n=1}^{N} |W_i(m, n)| \tag{2.16}$$

where W_i are the ith sub-band coefficients and $M \times N$ is the total number of coefficients in that sub-band. The feature vector is derived by concatenating the features at different scales and orientations as

$$E = [E_{1,1},\ E_{1,2},\ E_{1,3}, \ldots, E_{S,3},\ E_a]; \tag{2.17}$$

where S is the total number of scales and E_a is the energy of an approximate sub-band. The total number of sub-bands for THFB is $3S+1$. The derived feature vectors of each region are stored in the database as reference (enrollment process). The test iris pattern is classified on the basis of minimum Canbera distance (CD) between test iris feature vector and that of feature vectors stored in the database. The use of CD is due to the normalization property of individual feature components before computing the distance between test iris feature vector and that of databases. The CD is computed as

$$CD(X, Y) = \sum_{i=1}^{B} \frac{|X_i - Y_i|}{|X_i| + |Y_i|} \tag{2.18}$$

where B is the dimension of feature vector. X_i is the ith component of test feature vector and Y_i is ith component of enrolled feature vector.

2.4.2 Design of k-out-of-n:A Post-classifier for Iris Recognition

Iris recognition algorithms have succeeded in achieving a low FAR. However, reducing the FRR remains a major challenge. FRR needs to reduce to make iris recognition algorithm more robust. Many researchers have suggested that fusion of information extracted from classifiers provided better recognition performance as compared to single classifier [2, 4, 15, 39, 40]. In this work, fusion at the decision level is explored using *k-out-of-n:A* post-classifier. The value of k can be varied upto n and hence it is a flexible post-classifier. The designed post-classifier works on the ROC curve directly. ROC is the indirect representation of the distance scores between the test and enrolled feature vectors. ROC is obtained by varying threshold values of the distance scores. EER is a general optimal operating point that indicates threshold of the distance score. Multiple ROCs obtained from n-iris regions are fused by the post-classifier in order to improve the performance. The performance of the iris recognition system is assessed by measuring the errors made by rejecting genuine users (FRR), accepting impostor users for a given value of threshold (FAR), and computing computational complexity.

The test iris is accepted if at least any k out of the n-region(s) is (are) accepted (flexible *k-out-of-n:A*, where $k \leq n$). The details of general *k-out-of-n* system for the reliability analysis is given in [41]. In this rule, person is authenticated only when any k regions $k = 1, 2, 3$, and 4 out of n-regions ($n = 4$) passes the test of iris recognition. This system recognizes the person if any k distance scores (CDs) out of n-distance scores (CDs) are less than or equal to the corresponding thresholds.

FR can only occur by *k-out-of-n:A* post-classifier when n-regions iris tests produce FRs. Thus, genuine person is rejected when the combinations of k out of n-tests fail to recognize correctly. Based on this assumption, *k-out-of-n:A* post-classifier is framed for the different values of k as:

$$\begin{aligned}
FR &= \{CD_1^I > Th_1 \cap CD_2^I > Th_2 \ldots, \cap CD_n^I > Th_n\}, \quad k = 1. \\
FR &= \{(CD_1^I > Th_1 \cup CD_2^I > Th_2) \cap (CD_1^I > Th_1 \cup CD_3^I > Th_3) \\
&\qquad \ldots, \cap(\cdots \cup CD_n^I > Th_n)\}, \quad k = 2 \\
FR &= \{(CD_1^I > Th_1 \cup CD_2^I > Th_2 \cup CD_3^I > Th_3) \\
&\quad \cap (CD_1^I > Th_1 \cup CD_3^I > Th_3 \cup CD_4^I > Th_4) \\
&\qquad \ldots, \cap(\cdots \cup CD_n^I > Th_n)\}, \quad k = 3 \\
FR &= \{CD_1^I > Th_1 \cup CD_2^I > Th_2 \cup CD_3^I > Th_3 \cup CD_4^I > Th_4\}, \quad k = 4
\end{aligned} \tag{2.19}$$

where superscript I denotes the intra-class comparisons. The final fused FRR for $k = 1$ is computed by counting the number of CD_i^I greater than Th_i denoted as $C(CD_i^I, Th_i)$

$$FRR = \prod_{i=1}^{n} \frac{C(CD_i^I > Th_i)}{N_i} \tag{2.20}$$

where N is the total number of intra-class comparisons. Similarly, final FRRs are obtained for the different values of $k = 2, 3, 4$.

The FA occurs only if any k out of n-regions passes the test (k-CDs less than or equal to the corresponding thresholds). It is expressed as:

$$\begin{aligned}
FA &= \{CD_1^E \leq Th_1 \cup CD_2^E \leq Th_2 \ldots, \cup CD_n^E \leq Th_n\}, \quad k = 1. \\
FA &= \{(CD_1^E \leq Th_1 \cap CD_2^E \leq Th_2) \cup (CD_1^E \leq Th_1 \cap CD_3^E \leq Th_3) \\
&\quad \ldots, \cup(\cdots \cap CD_n^E \leq Th_n)\}, \quad k = 2 \\
FA &= \{(CD_1^E \leq Th_1 \cap CD_2^E \leq Th_2 \cap CD_3^E \leq Th_3) \\
&\quad \cup (CD_1^E \leq Th_1 \cap CD_3^E \leq Th_3 \cap CD_4^E \leq Th_4) \\
&\quad \ldots, \cup(\cdots \cap CD_n^E > Th_n)\}, \quad k = 3 \\
FA &= \{CD_1^E \leq Th_1 \cap CD_2^E \leq Th_2 \cap CD_3^E \leq Th_3 \cap CD_4^E \leq Th_4\}. \quad k = 4.
\end{aligned} \tag{2.21}$$

where superscript E denotes the inter-class comparisons. The final fused FAR for $k = 1$ is computed by counting CD_i^E less than or equal to Th_i denoted as $C(CD_i^E, Th_i)$

$$FAR = \sum_{i=1}^{n} \frac{C(CD_i^E \leq Th_i)}{Q_i} \tag{2.22}$$

where Q is the total number of inter-class comparisons. Similarly, final FARs are obtained for the different values of $k = 2, 3, 4$ (k of n-possible combinations). Through this process, the final fused FARs and FRRs are obtained separately for each value of k (fused ROC for each k from n-multiple ROCs).

2.5 Experimental Results

This section evaluates the proposed approach using UBIRIS [42], MMU1 [43], CASIA-IrisV2.0 (device1) [44], CASIA-IrisV3 (Interval) [44], and IITD [45] databases. The details of these databases have been provided in Appendix A. It is observed that segmentation on some of the images of all the databases is not accurate due to noncircular boundaries and poor transition from iris to sclera. Inaccurate segmented iris images are also used for the experimentation. Figure 2.7 shows few samples of inaccurately segmented images which were used for the experimentations. The combination of THFB and *k-out-of-n:A* has been compared with four successful existing iris recognition algorithms [1, 13–15]. In order to assess the recognition accuracy of fused post-classifier, the performance of THFB is compared for four different values of k.

In this chapter, to test the robustness of the proposed approach in the presence of artifacts, no preprocessing technique is used to isolate artifacts during iris recognition process. The scale and shift invariance are achieved by the normalization and

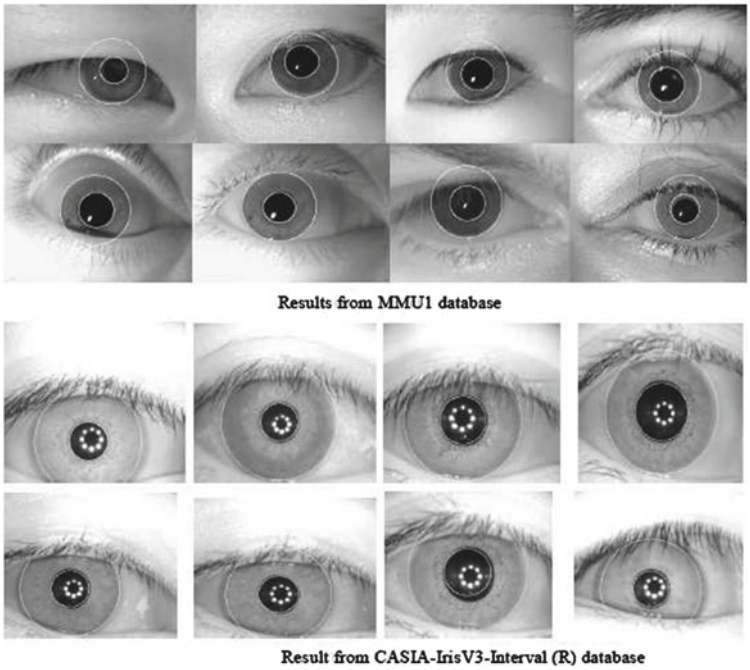

Fig. 2.7 Some inaccurate segmented images on MMU1 and CASIA-IrisV3-Interval databases

segmentation processes respectively. The registration process used two iris images per subject. To achieve rotation invariance, five normalized images corresponding to angles -10^0, -5^0, 0^0, 5^0, 10^0 are obtained from each image and used for training. Thus total number of enrolled images for each person is 10. For the testing, remaining three iris images per class are used. In no case images in training and testing sets are overlapping. In order to minimize the effect of intra-class variations and avail the discriminating iris information for the recognition, the upper half iris part from the original normalized iris image is selected. The selected half iris is partitioned into six sub-images and used four regions for the further processing. Each of these four regions is decomposed up-to two levels using these designed filters to create the four feature vectors separately. The artifacts present in iris images lead to reduction in accuracy. In order to improve the performance (reduce the error rate), *k-out-of-n:A* post-classifier is used on these four feature vectors. The performance of the proposed method (combination of THFB and *2-out-of-n:A*) has been compared with four existing well known iris recognition algorithms. These include Daugman [1], Monro et al. [13], Sun and Tan [14], and Dong et al. [15]. These algorithms are implemented and tested on the same set of normalized iris images for comparing the performance of this approach.

The first popular existing algorithm implemented for the comparison with the proposed approaches is the Daugman's algorithm [1]. In this algorithm, Gabor filters

Table 2.2 Comparison of the proposed technique (THFB + *k-out-of-n:A* ($k = 2$)) with existing iris recognition systems

Algorithms	UBIRIS		MMU1		CAS-IrisV2.0		CAS-IrisV3.0		IITD	
	FAR (%)	*FRR* (%)	*FAR* (%)	*FRR* (%)	*FAR* (%)	*FRR* (%)	*FAR* (%)	*FRR* (%)	*FAR* (%)	*FRR* (%)
Daugman	0.85	0.98	1.35	1.51	0.56	0.67	2.10	2.36	0.46	0.52
Sun and Tan	1.20	1.33	2.72	3.33	1.84	2.13	2.96	3.02	1.35	1.45
Monro et al.	2.29	3.11	4.64	5.56	3.59	4.27	5.16	5.11	2.98	3.01
Dong et al.	2.95	3.28	4.68	5.00	2.86	4.15	4.67	4.89	3.23	3.80
Proposed (k = 2)	0.52	0.49	1.99	1.89	0.36	0.41	1.91	2.10	0.16	0.15

are parameterized with four degrees-of-freedom: size of the kernels, orientations, and two positional co-ordinates (four scales and three orientations). They are applied on the specific regions of the normalized iris image in order to perform total 1,024 convolutions. The filter outputs of each region are quantized into two bits in order to obtain 2048 bits IrisCode. The dissimilarity between two IrisCodes is estimated using Hamming distance (without using a mask for separation of the region affected by artifacts). In second algorithm, dipole MLDF using 2-D Gaussian kernel (size—5×5 and $\sigma = 1.7$) [14] with $d = 5$ without using bootstrap method was implemented. The extension of this approach as suggested by Dong et al. [15], where the concept of personalized weight map is used for the robustness of encoding algorithm on different iris regions was implemented. It is observed that the robustness of the weight map depends upon the number of training images within a class. If number of training images within a class is more, the performance is significantly improved. This algorithm was trained using three training images per class. The next algorithm implemented is based on DCT coefficients and proposed in [13]. The experimental results for comparison of these algorithms have been presented in Table 2.2.

It is observed from Table 2.2 that the suggested method yields superior performance against these existing iris recognition methods. This is because it works on each selected region of iris independently, so artifacts can only affect the corresponding region and not the entire iris signature. The transformation on iris partitioned sub-regions does not corrupt the good iris region by combining them with artifacts (segmentation error, eyelids /eyelashes occluded regions, etc.). Thus, this approach achieves the robustness to intra-class variations (especially occlusion of pupil on iris due to inaccurate pupil segmentation, occlusion of eyelids/ eyelashes, specular reflection, etc.) in iris recognition system. Figure 2.8a–e shows the comparison in the form of ROC curve of the proposed method with state-of-the-art algorithms on UBIRIS, MMU1, CASIA-IrisV2.0 (device1), CASIA-IrisV3-Inerval, and IITD databases respectively. The influence of *k-out-of-n:A* post-classifier on the recognition performance of the suggested method was tested for different values of k. The experimental results are shown in Table 2.3.

It is observed that *2-out-of-4:A* post-classifier (acceptance of any two regions out of 4-regions) best suited for all the databases in order to improve the recognition

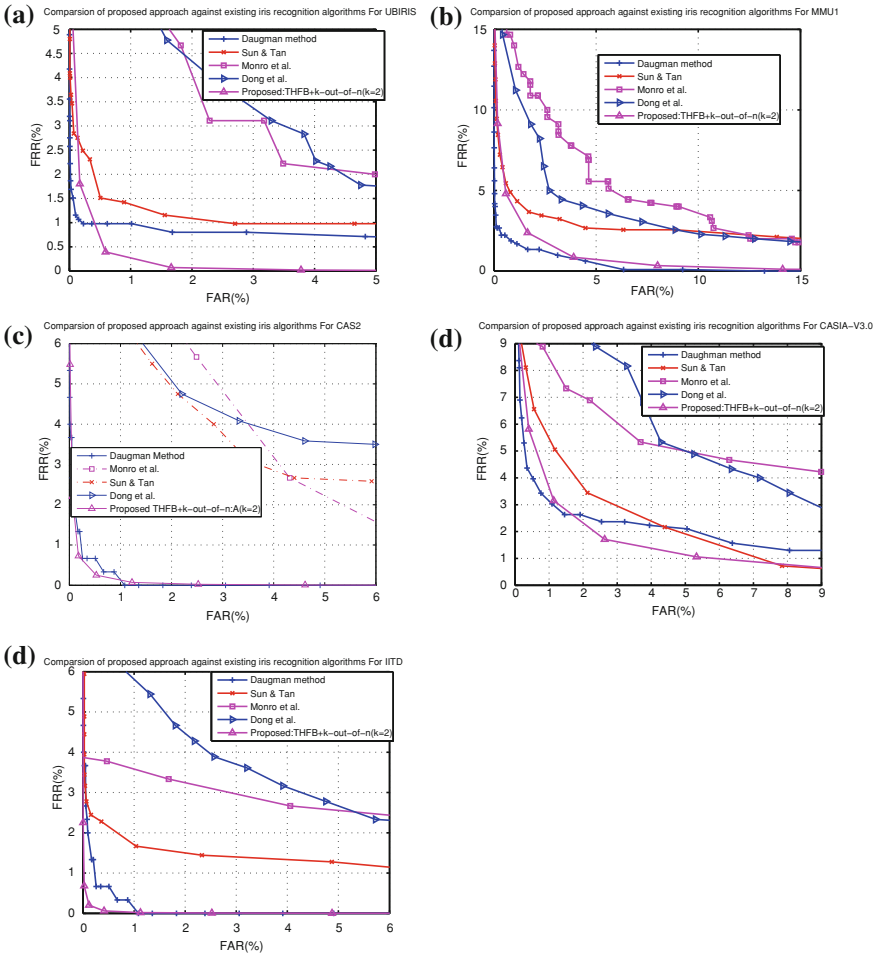

Fig. 2.8 Comparison of proposed algorithm with existing iris recognition algorithms using **a** UBIRIS **b** MMU1 **c** CASIA-IrisV2.0 **d** CASIA-IrisV3.0 **e** IITD iris databases

Table 2.3 Performance of proposed technique (THFB + *k-out-of-n:A*) for different values of k with $n = 4$

THFB + k-out-of-n:A	UBIRIS		MMU1		CAS-IrisV2.0		CAS-IrisV3.0		IITD	
	FAR (%)	*FRR* (%)	*FAR* (%)	*FRR* (%)	*FAR* (%)	*FRR* (%)	*FAR* (%)	*FRR* (%)	*FAR* (%)	*FRR* (%)
k = 1	2.47	2.76	4.45	4.56	1.96	2.03	2.47	2.76	0.92	0.98
k = 2	0.52	0.49	1.99	1.88	0.36	0.41	1.91	2.10	0.16	0.15
k = 3	0.48	0.53	2.38	2.61	0.42	0.46	1.48	1.53	0.30	0.35
k = 4	12.01	13.69	12.07	12.71	3.36	3.30	13.46	13.69	7.51	7.77

performance of the proposed method. The recognition performance of *4-out-of-4:A* is very poor. It is because this post-classifier has been selected all the four iris regions for the recognition which affect the performance due to the artifacts present on the normalized iris image. The detailed design of the FBs and iris recognition algorithms is given by authors in [46, 47].

2.6 Summary

In this chapter, a new class of separable 2-D biorthogonal wavelet basis is designed for iris feature extraction. The design is based on the generalized HBP and a class of THFB. First, three kernels are designed from the generalized halfband polynomial $P(z)$ by imposing the zeros at $z = -1$. These three designed kernels are used in three step ladder structure to obtain a new class of THFB by selecting the independent coefficients of the HBPs and the shape parameter p. The suggested approach has two degrees of freedom in the design compared to one in the existing THFB. The use of a class of THFB provides one more degree of freedom (p) by which we can shape better frequency response of the final filters. The desirable properties of the proposed FB for effective iris feature extraction are investigated. Also, flexible *k-out-n:A* post-classifier is incorporated on partitioned sub-images in order to reduce the FR. The developed method is robust against inaccurate pupillary and limbic boundary segmentations and is invariant to shift, scale, and rotation. The performance of the presented scheme is evaluated using five different databases and compared with four recently developed iris recognition algorithms. It is observed that cumulative effect of partition of normalized iris image, feature extraction using THFB, and exploration of *k-out-of-n:A* post-classifier significantly reduces error rates. The method provides low computational complexity which makes the technique feasible for online applications. The experimental results show that the performance of the proposed scheme under non-ideal environmental conditions (in presence of eyelids/eyelashes occlusion, inaccurate segmentation of inner and outer iris boundaries, specular reflection, etc.) is superior to recently developed iris recognition algorithms.

References

1. Daugman JG (1993) High confidence visual recognition of persons by a test of statistical independence. IEEE Trans Pattern Anal Mach Intell 25(11):1148–1161
2. Proença H, Alexandre LA (2007) Toward non-cooperative iris recognition: a classification approach using multiple signatures. IEEE Trans Pattern Anal Mach Intell 29(4):607–612
3. Masek L (2003) Recognition of human iris patterns for biometric identification. Master's thesis, Department of Computer Science and Software Engineering, The University of Western Australia
4. Vatsa M, Singh R, Noore A (2008) Improving iris recognition performance using segmentation, quality enhancement, match score fusion, and indexing. IEEE Trans Syst Man Cyber B

38(4):1021–1035
5. Boles WW, Boashash B (1998) A human identification technique using images of the iris and wavelet transform. IEEE Trans Signal Process 46(4):1185–1188
6. Wildes RP (1997) Iris recognition: an emerging biometric technology. Proc IEEE 85(9): 1348–1363
7. Lim S, Lee K, Byeon O, Kim T (2001) Efficient iris recognition through improvement of feture vector and classifier. ETRI 23((2)):61–70
8. Ma L, Tan T, Wang Y, Zhang D (2004) Personal identification based on iris texture analysis. IEEE Trans Pattern Anal Mach Intell 25(12):2519–2533
9. Ma L, Wang Y, Zhang D (2004) Efficient iris recognition by characterizing key local variations. IEEE Trans Image Process 13(6):739–750
10. Nabti M, Ghouti L, Bouridane A (2008) An effective and fast iris recognition system based on a combined multiscale feature extraction technique. Pattern Recogn 41:868–879
11. Velisavljević V (2009) Low-complexity iris coding and recognition based on directionlets. IEEE Trans Inf Forensic Secur 4(3):410–417
12. Abhyankar A, Schuckers S (2007) A novel biorthogonal wavelet network system for off-angle iris recognition. Pattern Recogn 43:586–594
13. Monro DM, Rakshit S, Zhang D (2007) DCT based iris recognition. IEEE Trans Pattern Anal Mach Intell 29(4):586–595
14. Sun Z, Tan T (2009) Ordinal measures for iris recognition. IEEE Trans Pattern Anal Mach Intell 31(12):2211–2226
15. Dong W, Tan T, Sun Z (2010) Iris matching based on personalized weight map. IEEE Trans Pattern Anal Mach Intell 99(1):1–14
16. Kumar A, Passi A (2010) Comparison and combination of iris matchers for reliable personal authentication. Pattern Recogn 43(3):1016–1026
17. Huang J, You X, Yuan Y, Yang F, Lin L (2010) Rotation invariant iris feature extraction using Gaussian Markov random fileds with non-seprable wavelet. Neurocomputing 73:883–894
18. Park C, Lee J, Oh S, Song Y (2003) Iris feature extraction and matching based on maltiscale and directional image representation. In: Proceedings of 4th international conference on scale space methods in computer vision, Isle of Skye, UK, 2003, Springer-Verlag, pp 576–583
19. Patil B, Patwardhan P, Gadre V (2008) On the design of fir wavelet filter banks using factorization of a halfband polynomial. IEEE Signal Process Lett 15:485–488
20. Daubechies I (1992) Ten lectures on wavelets. SIAM, Philadelphia
21. Daubechies I, Feauveau J (1992) Biorthogonal bases of compactly supported wavelets. Commun Pure Appl Math 45:485–560
22. Ansari R, Kaiser CGJ (1991) Wavelet construction using Lagrange halfband filters. IEEE Trans Circuits Syst Express Brief 38(9):1116–1118
23. Sweldens W (1996) The lifting scheme: a custom-design construction of biorthogonal wavelets. Appl Comput Harmonic Anal 3(2):186–200
24. Phoong S, Kim C, Vaidyanathan P, Ansari R (1995) A new class of two-channel biorthogonal filter banks and wavelet bases. IEEE Trans Signal Process 43(3):649–665
25. Ansari R, Kim C, Dedovic M (1999) Structure and design of two-channel filter banks derived from a triplet of halfband filters. IEEE Trans Circuits Syst II Analog Digital Signal Process 46(12):1487–1496
26. Tay DBH, Palaniswami M (2004) A novel approach to the design of the class of triplet halfband filterbanks. IEEE Trans Circuits Syst Syst II Express Brief 51(7):378–383
27. Tay DBH (2008) ETHFB: A new class of even-length biorthogonal wavelet filters for Hilbert pair design. IEEE Trans Circuits Syst Syst I Regul Pap 55(6):1580–1588
28. Chan S, Yeung K (2004) On the design and multiplierless realizaton of perfect reconstruction triplet-based fir filterbanks and wavelet bases. IEEE Trans Circuits Syst Syst I 51(8): 1476–1491
29. Kha H, Tuan H, Nguyen T (2011) Optimal design of fir triplet halfband filter bank and application in image coding. IEEE Trans Image Process 22(2):586–591

30. Eslami R, Radha H (2010) Design of regular wavelets using a three-step lifting scheme. IEEE Trans Signal Process 58(4):2088–2101
31. Kovacevic J, Sweldens W (2000) Wavelet families of increasing order in arbitrary dimensions. IEEE Trans Image Process 9(3):480–496
32. Strang G, Nguyen T (1996) Wavelets and filter banks. Wellesley-Cambridge, NY
33. Vetterli M, Kovacevic J (1995) Wavelets and subband coding. Prentice-Hall, Englewood Cliffs
34. Mojsilovic A, Popovic M, Rackov D (2008) On the selecton of optimal wavelet basis for texture characterization. IEEE Trans Image Process 9(12):2043–2050
35. Vaidyanathan PP (1993) Multirate systems and filter banks. Prentice-Hall, Englewood Cliffs
36. Tay DBH (2001) Balanced spatial and frequency localized 2-D nonseparable wavelet filters. In: Proceedings of IEEE international symposium on circutis and systems, May 2001, vol 2, pp 489–492
37. Monro D, Sherlock B (1997) Space frequency balance in biorthogonal wavelets. In: Proceedings of IEEE international conference on image processing, October 1997, vol 1, pp 642–627
38. Chen Y, Dass S, Jain A (2006) Localized iris image quality using 2-D wavelets. In: Proceedings of international conference on biometrics, 2006, pp 373–381
39. Ross A, Jain A (2003) Information fusion in biometrics. Pattern Recogn Lett 24(13): 2115–2125
40. Daugman JG (2000) Biometric decision landscapes. University of Cambridge, Technical Report
41. Ebeling E (1997) An introduction to reliability and maintability engineering. McGraw-Hill, International edition, New York
42. Proenca H, Alexandre L. UBIRIS: a noisy iris image database. www.iris.di.ubi.pt
43. Multimedia University (2004) MMU iris image database. http://pesona.mmu.edu.my/ccteo
44. CASIA iris image database. http://www.sinobiometrics.com/casiairis.htm
45. IITD iris image database. http://web.iitd.ac.in
46. Rahulkar AD, Holambe RS (2012) Half-iris feature extraction and recognition using a new class of biorhtogonal triplet half-band filter band and flexible k-out-of-n:A. Postclassifier. IEEE Trans Inf Forensic Secur 7(1):230–240
47. Rahulkar AD, Patil BD, Holambe RS (2012) A new approach to the design of biorthogonal triplet halfband filter banks using generalized halfband polynomials. Signal Image Video Process (Springer) 1–12

http://www.springer.com/978-3-319-06766-7

Iris Image Recognition
Wavelet Filter-banks Based Iris Feature Extraction Schemes
Rahulkar, A.D.; Holambe, R.S.
2014, XIII, 84 p. 33 illus., 17 illus. in color., Softcover
ISBN: 978-3-319-06766-7